Application of Conditional Nonlinear Optimal Perturbation to Targeted Observation Studies of the Atmosphere and Ocean

MU Mu[1] (穆 穆), WANG Qiang[1*] (王 强), DUAN Wansuo[2] (段晚锁), and JIANG Zhina[3] (姜智娜)

1 *Key Laboratory of Ocean Circulation and Waves, Institute of Oceanology, Chinese Academy of Sciences, Qingdao* 266071

2 *State Key Laboratory of Numerical Modeling for Atmospheric Sciences and Geophysical Fluid Dynamics, Institute of Atmospheric Physics, Chinese Academy of Sciences, Beijing* 100029

3 *State Key Laboratory of Severe Weather, Chinese Academy of Meteorological Sciences, Beijing* 100081

(Received March 13, 2014; in final form July 11, 2014)

ABSTRACT

This paper reviews progress in the application of conditional nonlinear optimal perturbation to targeted observation studies of the atmosphere and ocean in recent years, with a focus on the El Niño–Southern Oscillation (ENSO), Kuroshio path variations, and blocking events. Through studying the optimal precursor (OPR) and optimally growing initial error (OGE) of the occurrence of the above events, the similarity and localization features of OPR and OGE spatial structures have been found for each event. Ideal hindcasting experiments have shown that, if initial errors are reduced in the areas with the largest amplitude for the OPR and OGE for ENSO and Kuroshio path variations, the forecast skill of the model for these events is significantly improved. Due to the similarity between patterns of the OPR and OGE, additional observations implemented in the same sensitive region would help to not only capture the precursors, but also reduce the initial errors in the predictions, greatly increasing the forecast abilities. The similarity and localization of the spatial structures of the OPR and OGE during the onset of blocking events have also been investigated, but their application to targeted observation requires further study.

Key words: conditional nonlinear optimal perturbation, targeted observation, ENSO, Kuroshio path variations, blocking

Citation: Mu Mu, Wang Qiang, Duan Wansuo, et al., 2014: Application of conditional nonlinear optimal perturbation to targeted observation studies of the atmosphere and ocean. *J. Meteor. Res.*, **28**(5), 923–933, doi: 10.1007/s13351-014-4057-8.

1. Introduction

During the early development of numerical weather prediction, meteorologists noticed that the forecast skill in a focused area was limited by the initial conditions in a local region (Riehl et al., 1956). The improvement in forecast skill from adding observations in a local area may be no less than that induced by addition of the observations in a wide area. This idea of adding additional observations in a local area to improve the forecast ability, is called targeted observation, or adaptive observation. To make a more accurate prediction at a future verification time ($t_{\rm v}$) in a focused verification area, additional observations are implemented at a future targeted time ($t_{\rm a}$), where $t_{\rm a} < t_{\rm v}$, in a sensitive area where the observations are expected to have a great impact on the forecasts in the verification area, as shown in Fig. 1. The additional observations are assimilated by data assimilation system to provide a more reliable initial state for the model. A detailed description of targeted observation can be found in Mu (2013).

The theory and practice of numerical weather prediction and climate projection indicate that, aside from the performance of numerical prediction models, successful forecasting depends on the quality of the

Supported by the National Natural Science Foundation of China (41230420 and 41306023) and China Meteorological Administration Special Public Welfare Research Fund (GYHY201306018).

*Corresponding author: wangqiang@qdio.ac.cn.

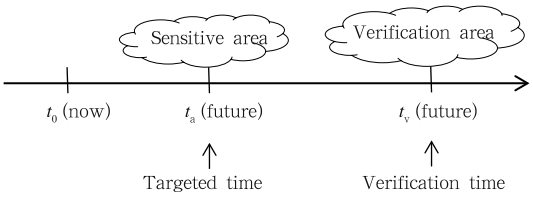

Fig. 1. Schematic diagram of targeted observation. [From Mu et al., 2012]

initial field. In particular, if the initial field contains signals of the occurrence and development of the focused event, the amplitude of the initial error significantly affects the forecast. The key idea of targeted observation, denoted as region A, is to look for the sensitive area of initial error. However, the sensitive area of the precursor for the occurrence of an anomaly event, denoted as region B, should also be investigated. Intuitively, region A should contain region B; however, these two regions may be significantly different upon further inspection. In this situation, although the targeted observation implemented in region A could reduce the forecast error, the forecast skill may be still relatively low because the signals are not well captured. However, if regions A and B are almost the same, the targeted observation carried out in a local area can not only find the precursor, but also reduce the initial error. This helps to improve the accuracy of the forecast and save on the huge costs caused by the observation. Interestingly, Mu Mu and his group have found and proved that the two regions are almost the same when studying the predictabilities of the atmospheric and oceanic anomaly events such as the El Niño–Southern Oscillation (ENSO), Kuroshio path variations, and atmospheric blocking (Mu and Jiang, 2011; Wang et al., 2013; Mu et al., 2014). This result is a solid foundation for targeted observations of the above events.

In the studies mentioned above, the conditional nonlinear optimal perturbation (CNOP; Mu et al., 2003) approach was used. CNOP represents the initial perturbation that attains the largest nonlinear evolution at the prediction time. Because the linear approximation assumption is not used, the CNOP method can be considered an extension of the singular vector (LV) method in the nonlinear regime (Duan and Mu, 2009), and sufficiently represents the roles of nonlinear dynamics and physical processes. Here, we review the use of the CNOP method in studies of the optimal precursor (OPR) and optimally growing initial error (OGE) in the predictability of the ENSO, Kuroshio path variations, and atmospheric blocking. The OPR refers to the initial anomaly that most easily develops into some weather or climate events under specific conditions, while the OGE represents the initial error with the largest nonlinear evolution that results in a non-negligible forecast error. It has been found that the spatial patterns of the OPR and OGE are highly similar and have obvious localization characteristics for each anomaly event (Mu and Jiang, 2011; Wang et al., 2013; Mu et al., 2014). This means that additional observations over the sensitive area identified based on the similarity and localization features can well capture the precursor signal and reduce the initial error, thus improving the forecast skill.

The CNOP method has been successfully used to determine the sensitive areas of typhoon and heavy rain. For example, Mu et al. (2009) and Qin and Mu (2011) have used the method to recognize the sensitive area of a typhoon. Wang and Tan (2009) and Tan et al. (2011) developed a fast algorithm to calculate the CNOP and determined the sensitive area for the prediction of a typhoon. In addition, Liu et al. (2013) employed the CNOP method to identify the sensitive area for the targeted observation of a winter storm in the middle-lower branches of the Yangtze River. These studies have been reviewed in Mu (2013); hence, we omit reviewing them here. The present paper will mainly summarize the obtained results about OPR and OGE in the predictability studies of ENSO, Kuroshio path variations, and atmospheric blocking during recent years, and particularly focus on the similarity and localization characteristics of the spatial structures of OPR and OGE and associated inspiration to the determination of the sensitive area of targeted observation, so as to provide scientific basis for the implementation of the targeted observation of the aforementioned anomaly events.

2. Sensitive area for the prediction of El Niño

The roles of initial errors in ENSO predictability

have been investigated by many researchers. For example, Moore and Kleeman (1996) and Xue et al. (1997) suggested that ENSO prediction is sensitive to the initial condition. Chen et al. (2004) indicated that the spring predictability barrier (SPB) of ENSO can be greatly overcome through improvement of the initialization for the Zebiak-Cane model (Zebiak and Cane, 1987). Recently, Mu et al. (2007a, b) and Duan et al. (2009) demonstrated that ENSO predictions are closely associated with the growth of initial errors resulted from nonlinear instability, and emphasized that the initial errors with particular structures could cause the prominent SPB. Furthermore, Duan and Zhang (2010) and Yu et al. (2012a) showed the importance of initial errors by comparing them with the model parameter errors. If the initial errors of a particular pattern could be filtered and more accurate initial fields obtained, the prediction skill of the model for the ENSO may be well improved. Targeted observation may be one of the approaches that can filter out those initial errors (Duan and Mu, 2009; Yu et al., 2009).

Mu et al. (2007b) used the Zebiak-Cane model to investigate the initial error and found that the CNOP method represented the initial error that had the largest effect on the ENSO prediction, namely, the OGE, which could yield a significant SPB for El Niño events. They also argued that although some other initial errors had the same magnitude as the CNOPs, these errors neither caused significant prediction uncertainties nor yielded apparent season-dependent evolution, and therefore failed to induce SPB for El Niño events. It is clear that a particular error pattern is necessary for the occurrence of SPB for El Niño events. Yu et al. (2009) further divided the CNOP-type initial error into two types using cluster analysis (Fig. 2). The first type of CNOP error (termed type-1 OGE) possessed a thermocline depth anomaly component with a deepening along the equator, and an SSTA structure with negative anomalies in the equatorial central to western Pacific and positive anomalies in the equatorial eastern Pacific. The other type

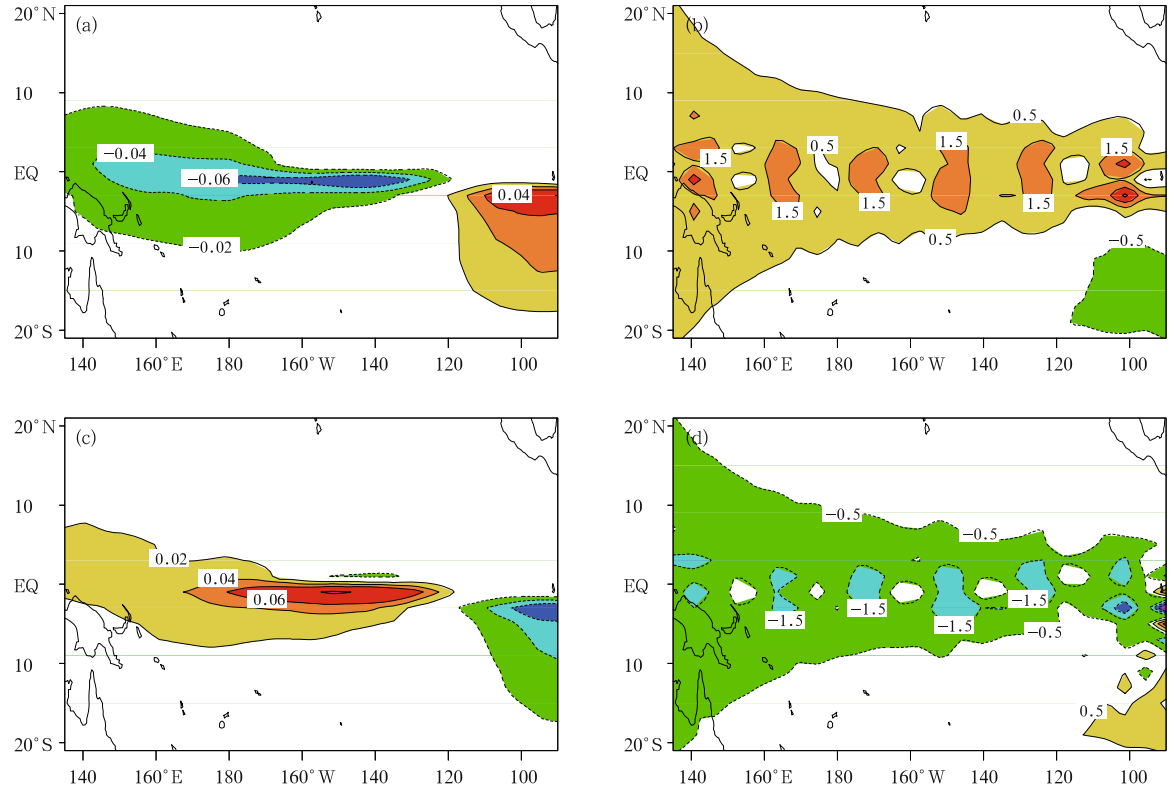

Fig. 2. (a, b) Type-1 and (c, d) type-2 OGEs for El Niño events in the Zebiak-Cane model. (a, c) The sea surface temperature anomaly (SSTA) and (b, d) the thermocline depth anomaly. [From Yu et al., 2009]

(type-2 OGE) possessed a sign almost opposite to the former. Although the two OGEs had different patterns, they were both associated with a localized region, so predictions may be sensitive to this.

On the other hand, the CNOP also played a role in the OPRs for El Niño and La Niña events (Fig. 3). Duan et al. (2013) calculated the CNOP-type initial anomaly and found that the OPR for El Niño is similar to the type-1 OGE of El Niño, namely, it possesses an SSTA dipole over the equatorial central and eastern Pacific, plus positive thermocline depth anomalies over the entire equatorial Pacific. Mu et al. (2014) also found that the OPR for La Niña is similar to the type-2 OGE. Hence, Mu et al. (2014) suggested that the OPR and OGE for El Niño share great similarities, localization, and evolution mechanisms. Thus, if additional observation instruments are deployed as targeted observation with limited coverage, the similarly large amplitude areas for the OPR and OGE should be considered first, to better detect the early signals for ENSO events and meanwhile reduce the initial errors. The identified area may also represent the sensitive area for ENSO prediction.

To test the validity of the aforementioned sensitive area, Yu et al. (2012b) divided the tropical Pacific into six parts with equal numbers of grid points (Fig. 4). Domain 5 covers the equatorial central and eastern Pacific and has the large amplitude area of both the OPR and OGE for El Niño events. For each domain, the CNOP-type initial error was computed and the maximum prediction error caused by the initial error was checked. It is found that the initial error in Domain 5 evolved more significantly than those in other domains. This reflected the fact that the SST initial errors over the equatorial central and eastern Pacific may have the biggest effect on El Niño prediction.

Yu et al. (2012b) further investigated the effects of the sensitive area on the improvement of ENSO forecast skill using 240 initial analysis fields obtained from hindcasting experiments from January 1980 to December 1999 with a later version of the Zebiak-Cane model (Chen et al., 2004). They replaced the initial analysis field in each of the six domains with the initial field of the El Niño event to eliminate the error of the initial field for each domain, and examined the reduction of forecast error (Fig. 5). They found that the decrease in the prediction error was more significant when eliminating the initial error in domain 5 than in the other domains.

3. Sensitive area for the prediction of Kuroshio path variations

The Kuroshio path variation south of Japan is a key problem in physical oceanography. Some researchers have attempted to predict the Kuroshio path

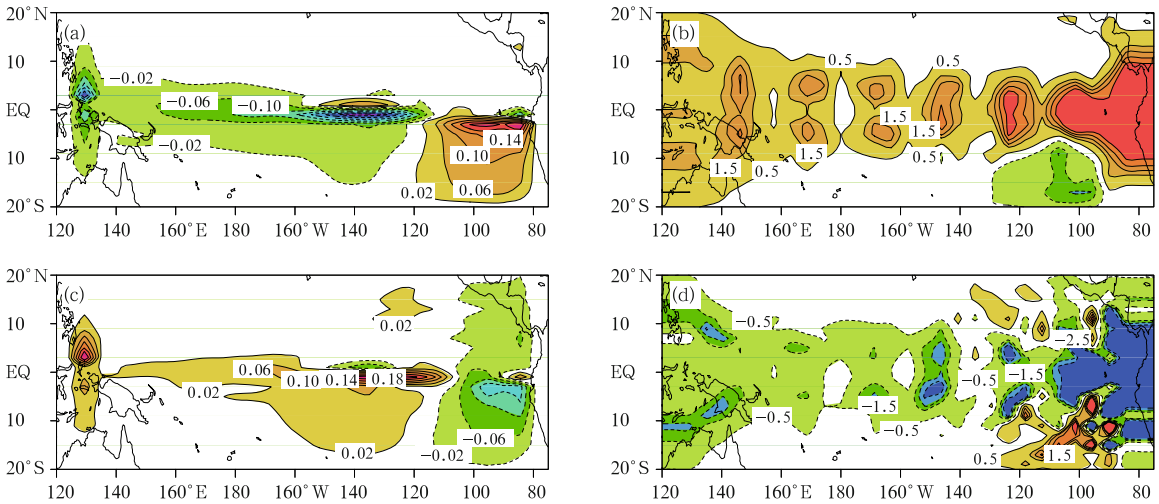

Fig. 3. OPRs for (a, b) El Niño and (c, d) La Niña. (a, c) The SSTA and (b, d) the thermocline depth anomaly. [From Mu et al., 2014]

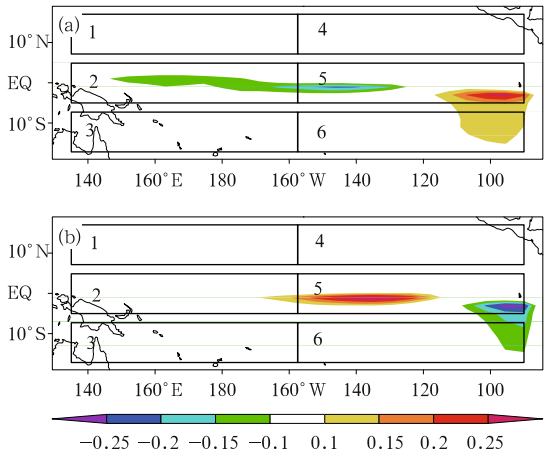

Fig. 4. Two kinds of CNOP initial errors: (a) type-1 and (b) type-2, over the tropical Pacific divided into six regions labeled as domains 1–6. Large values of both kinds of errors occur mainly in domain 5. [From Yu et al., 2012b]

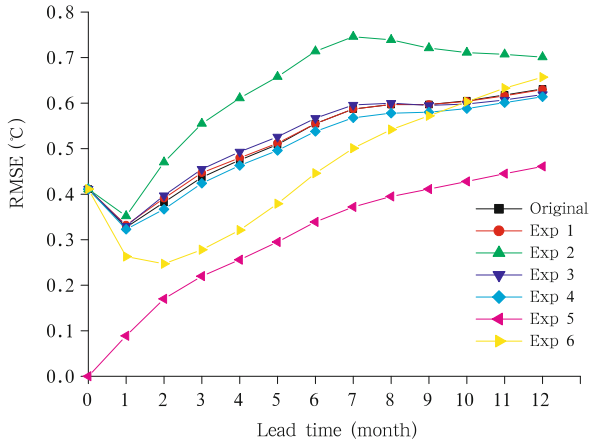

Fig. 5. Root mean square errors for the Niño-3 SSTA caused by the original initial errors (squares connected by a black line) and six other sets of initial errors (labeled Exps. 1–6). Each set of new initial errors was generated by eliminating errors in one of the six domains (Fig. 4) from the original initial errors. [From Yu et al., 2012b]

variations because they have important effects on climate change, marine environment, and fisheries (Komori et al., 2003; Kamachi et al., 2004; Miyazawa et al., 2005; Usui et al., 2006; Wang et al., 2012). Similar to the above ENSO predictability studies, Wang et al. (2013) utilized the CNOP method to explore the OPR and OGE of Kuroshio path variations, and also found that the spatial patterns of the OPR and OGE shared great similarities and obvious localization features.

Wang et al. (2013) employed the CNOP approach to investigate the OPR of the occurrence of Kuroshio large meander within a 1.5-layer shallow-water model. Figure 6a shows the upper-layer thickness component of the OPR and indicates that the spatial structures of the OPR shared obvious localization characteristics and its large amplitude area was mainly located in the upstream region of the Kuroshio large meander. Through investigating the evolution of the OPR, they found that the advection of potential vorticity played a vital role in the formation of the large meander path. Simultaneously, they also calculated the OGEs for the prediction of Kuroshio path variations. The OGEs were divided into two types: type-1 and type-2 OGEs, as shown in Figs. 6b and 6c. It can be seen that the OPR was similar to the two types of OGEs: the similarity coefficient between the OPR and type-1 (type-2) OGE was negative (positive). They further found that the evolution process of the type-1 OGE was negatively correlated with that of OPR, resulting in the strength of the forecasted large meander path to be underestimated. On the contrary, the evolution of the type-2 OGE was positively correlated with that of OPR, causing the amplitude of the forecasted large meander to be overestimated. These results reflect that the evolution mechanisms of the OPR and OGE were similar.

The similarity and localization features of the OPR and OGE inspired the above targeted observation studies of Kuroshio path variations. To determine the sensitive area, Wang et al. (2013) computed the total energy distributions of the type-1 OGE (Fig. 7). Because the spatial structures of the OPR and OGEs were similar, the total energy distributions of the OPR and type-2 OGE were almost the same as those of the type-1 OGE. Figure 7 illustrates that the large amplitude regions of the total energy of the type-1 OGE were mainly located to the southeast of Kyushu. Hence, the sensitive area was defined as a box, denoted as R3 in Fig. 7, big enough to contain the large amplitude of the total energy.

To examine the validity of the sensitive area, Wang et al. (2013) investigated the evolution of initial

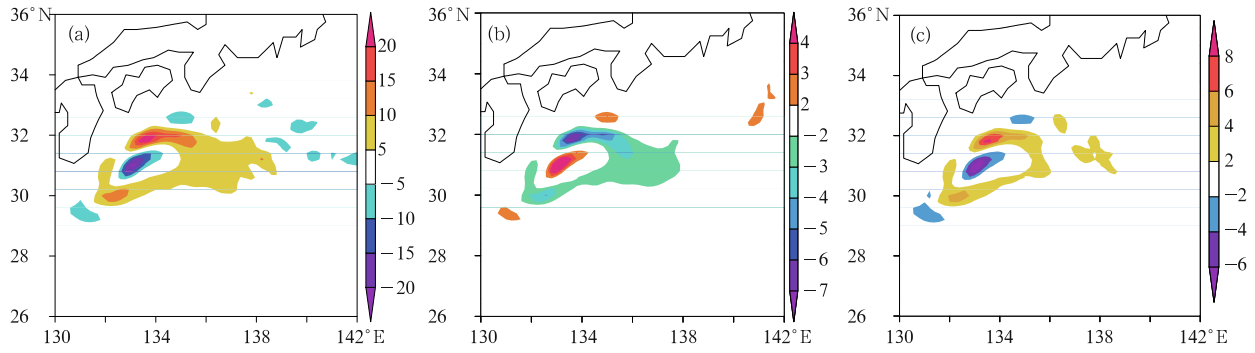

Fig. 6. The upper-layer thickness component of the OPR (a) for the Kuroshio large meander, and (b) type-1 and (c) type-2 OGEs in prediction of the large meander path (m). [From Wang et al., 2013]

random errors in different areas. Figure 7 shows nine local regions with the same size (240 grid points), including the sensitive area R3 and eight other arbitrarily chosen regions. These regions mainly cover the south of Japan and upstream of the Kuroshio extension. Forty random error fields were generated for each region. The generation process was follows: first, a random sequence with a normal distribution of variance σ_{ij} was generated, where i and j denote the variables in the 1.5-layer shallow-water model and the grid point, respectively. The random sequence was denoted as $N(0, \sigma_{ij})$, where i has the range 1–3 and j = 1–240. A random number selected from $N(0, \sigma_{ij})$ was regarded as the random error for the variable i at the grid point j, creating a random error field for each region. To compare the evolution of the random error and the type-1 OGE, Wang et al. (2013) scaled the random error field, x_r, so that its total energy equals that of the type-1 OGE. The average kinetic energy of the forecast errors caused by the random errors is listed in Table 1 for each region. These results show that the evolution of the initial errors depends on their locations. The forecast error caused by the error in the sensitive area R3 is the largest.

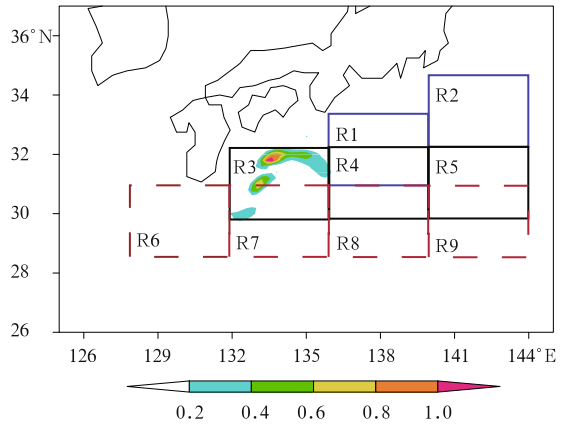

Fig. 7. Spatial structure of the total energy for type-1 OGE (shaded; m^3 s^{-2}). The nine regions were used for the ideal targeted observation experiments, and R3 was the sensitive area. The locations of these nine regions are listed in Table 1. [From Wang et al., 2013]

To investigate whether the targeted observations implemented over the sensitive area R3 improved the forecast skill of Kuroshio path variations, Wang et al. (2013) performed the following hindcasting experiments. First, 40 random initial errors over the whole model domain were obtained with the same amplitude as the type-1 OGE. The averaged kinetic energy of the forecast errors caused by the random errors was denoted J_1. Second, the additional observations were carried out for one of the nine regions, and so the random errors within that region were eliminated, with-

Table 1. Average values of kinetic energy of the forecast errors obtained from evolution of 40 random initial errors in each region (Wang et al., 2013)

Region	Location	Average kinetic energy ($\times 10^9$ m^5 s^{-2})
R1	(31.0°–33.4°N, 136°–140°E)	9.6
R2	(32.2°–34.6°N, 140°–144°E)	3.1
R3	(29.8°–32.2°N, 132°–136°E)	26.0
R4	(29.8°–32.2°N, 136°–140°E)	9.6
R5	(29.8°–32.2°N, 140°–144°E)	4.7
R6	(28.6°–31.0°N, 128°–132°E)	1.7
R7	(28.6°–31.0°N, 132°–136°E)	7.6
R8	(28.6°–31.0°N, 136°–140°E)	6.5
R9	(28.6°–31.0°N, 140°–144°E)	2.7

out changing the errors outside of that region (Fig. 7). As a result, 40 random initial error fields were obtained for each region. The average kinetic energy of the prediction errors caused by the evolution of these random error fields was denoted J_2. The improvement of the prediction due to the implementation of targeted observations was measured with the metric $(J_2 - J_1)/J_1$, where a negative number indicates a decrease of the forecast error. Table 2 shows the relative differences of the forecast errors for different areas. The reduction of the forecast error corresponding to the sensitive area is 43.59%, the largest among all the regions. This implies that if targeted observations were implemented over the sensitive area, the initial condition in this region would improve, and the precursor signal of the occurrence of the Kuroshio path variations would be well captured, greatly improving the forecast skill of the Kuroshio path variations.

Table 2. Relative differences of the average kinetic energy of the forecast errors with and without implementing the targeted observations (Wang et al., 2013)

Region	R1	R2	R3	R4	R5	R6	R7	R8	R9
Relative differences (%) of forecast errors	–15.28	–1.68	–43.59	–11.85	–26.70	–0.04	–1.25	–1.53	0.73

4. Sensitive area for the prediction of atmospheric blocking

Blocking is a typical large-scale system, which has a deep impact on the regional weather and climate (Rex, 1950). Blocking prediction is extremely sensitive to the initial conditions, which leads to a limited forecast skill. Therefore, improvement of the forecast skill of blocking events is one of the key problems of medium-to-long term numerical weather forecasting (Tibaldi and Molteni, 1990; Kimoto et al., 1992; Frederiksen et al., 2004). We tried to assess whether blocking events shared the great similarity between OPR and OGE, as found for the ENSO and Kuroshio path variations.

Jiang and Wang (2010) calculated the OPR for the Euro–Atlantic blocking with the CNOP method, based on a T21L3 quasi-geostrophic spectral model (Marshall and Molteni, 1993). Figure 8 presents OPR as a baroclinic northeast-southwest oriented wave train over the North American continent, which is westward with height over the northward side of the Atlantic jet. In addition, the OPR displays localization characteristics in its spatial distribution. With time, the OPR propagated downward and amplified into a dipole blocking pattern over the Euro–Atlantic region. The energy source of the OPR evolution mainly came from the horizontal shear of the basic state, and less from the baroclinic adjustment.

Mu and Jiang (2011) explored the OPR and OGE based on 20 cases from 1985 to 1991. The composite evolution of the OPR (Fig. 9) shows that the OPR was a wave train upstream of the blocking region. With time, it propagated downward and amplified to become a high-over-low dipole structure. The OGE had two types: type-1 OGE was a local CNOP while type-2 OGE was a global CNOP. With an optimization time of 3 days, the similarity coefficient between the OPR and type-1 OGE was 0.95, while that between the OPR and type-2 OGE was –0.87. When the optimization time was extended to 4 days, the similarity reduced. The similarity coefficient between the OPR and type-1 OGE was 0.85, and between OPR and type-2 OGE was only –0.69. As to the temporal evolution, the OPR had similar characteristics to the type-1 OGE, and developed into a high-over-low dipole pattern. Type-2 OGEs also showed similar behavior, but with an opposite sign to blocking. In conclusion, OPR and OGE in blocking had similar spatial patterns, and similar evolutionary behavior.

Though a blocking event is an atmospheric process, the similarity between the OPR and OGE, and the localization characteristics appearing in the ENSO and Kuroshio path variations were also found in blocking processes. Therefore, by applying targeted observation in the sensitive region identified by the OGE, we can reduce the possibility of OGE, capture the signal of the OPR, and improve the forecasting of a block-

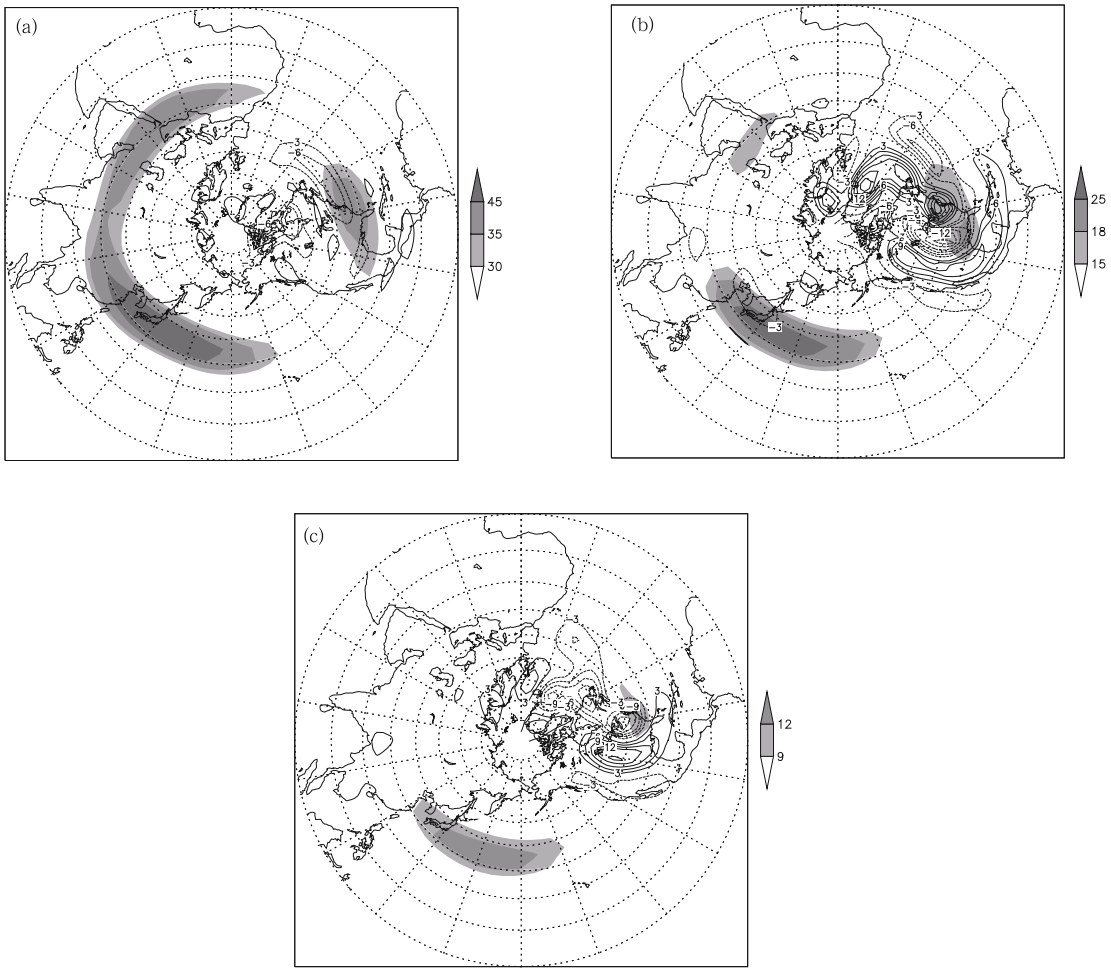

Fig. 8. OPR (contours; gpm) of Euro–Atlantic blocking for an optimization time of 3 days, and the climatological zonal wind (shaded; m s^{-1}) over a 20-yr integration period from 1 December 1983 at (a) 200, (b) 500, and (c) 800 hPa. [From Jiang and Wang, 2010]

ing event. The validity of the targeted observation in blocking forecasting should be tested by using observation simulation system experiments.

5. Summary and discussion

This paper has reviewed the applications of the CNOP method to targeted observation studies of the ENSO, Kuroshio path variations, and atmospheric blocking, while emphasizing the similarity between the OPR and OGE and its applications to identifying the sensitive areas of the targeted observations of the events mentioned above. Specifically, the OGEs of the ENSO, Kuroshio path variations, and atmospheric blocking are all located in some specific areas. The localization areas of these OGEs may represent the sensitive areas of the targeted observation. Through ideal hindcasting experiments using targeted observation studies of the ENSO and Kuroshio path variations, we proposed that additional observations in the sensitive areas can help to improve forecast skills. As for atmospheric blocking, further numerical experiments are needed to investigate whether targeted observation in the sensitive areas would improve the related forecast skill.

Moreover, this paper has stressed the similarity between the OPR and OGE in the above events and their spatial localization characteristics, which can

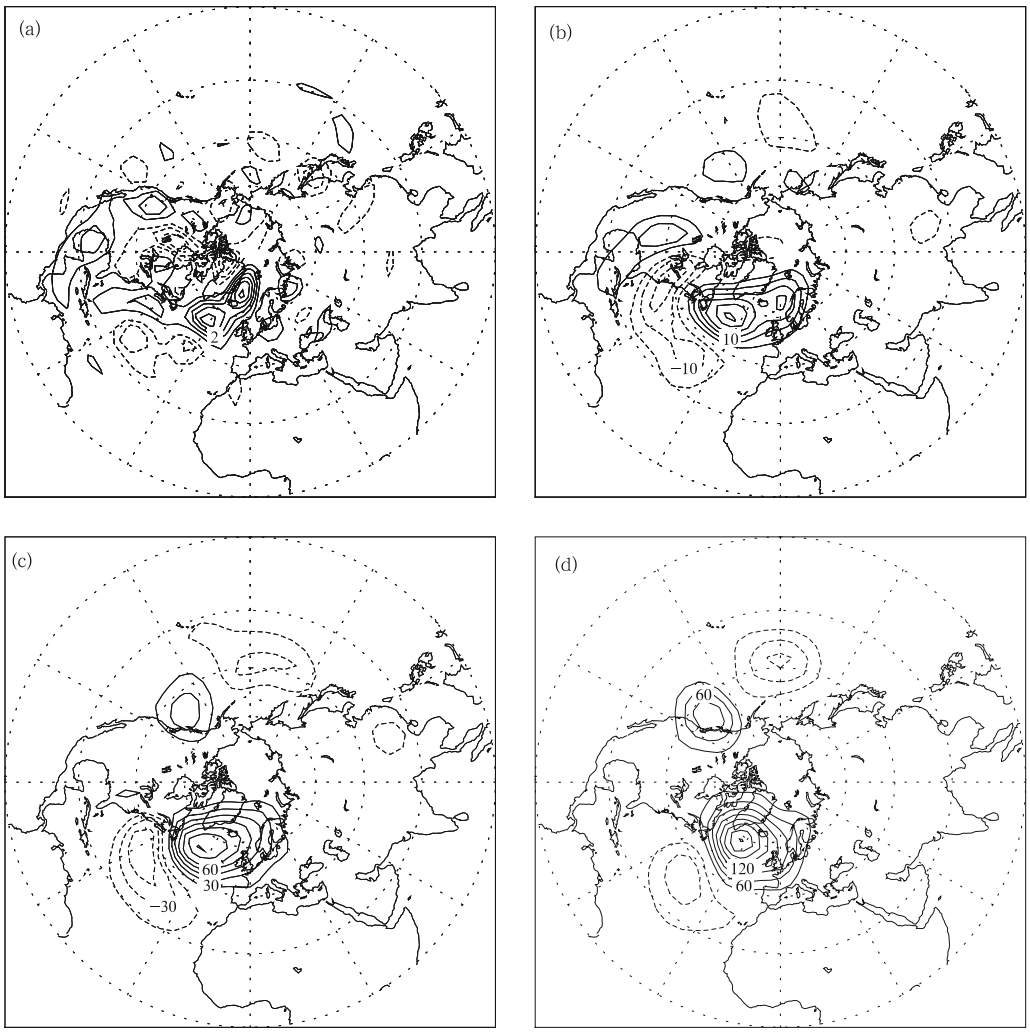

Fig. 9. Composite nonlinear evolution of the OPR (gpm) for 20 cases at 500 hPa on (a) day 0, (b) day 1, (c) day 2, and (d) day 3. [From Mu and Jiang, 2011]

provide useful information for the implementation of targeted observation. If targeted observations are implemented in sensitive areas determined by the OGE, the probability of the appearance of the OGE can be eliminated, which can improve initial fields and reduce the prediction errors. Additionally, this method can provide better guidance for building a local observation network, helping to capture OPR signals easily and increasing forecasting ability. The above results have illustrated that the similarity and spatial localization features of the OPR and OGE are of great importance for targeted observation. Are these features associated with most atmospheric and oceanic anomaly events? In order to answer this question, the OPR and OGE similarity and spatial localization for different anomaly events should be investigated.

Targeted observation studies of atmospheric and oceanic anomaly events are challenging. However, with the rising capabilities of computers, effective multidisciplinary study, and collaboration of researchers from different fields, progress in this field is likely contributing and will contribute to the improvement of the prediction of weather and climate.

REFERENCES

Chen, D., M. Cane, A. Kaplan, et al., 2004: Predictability of El Niño over the past 148 years. *Nature*, **428**,

733–736.

Duan, W. S., X. C. Liu, K. Y. Zhu, et al., 2009: Exploring the initial errors that cause a significant "spring predictability barrier" for El Niño events. *J. Geophys. Res.*, **114**, C04022, doi: 10.1029/2008JC004925.

——, Y. S. Yu, H. Xu, et al., 2013: Behaviors of nonlinearities modulating the El Niño events induced by optimal precursory disturbances. *Climate Dyn.*, **40**, 1399–1413.

Duan Wansuo and Mu Mu, 2009: Conditional nonlinear optimal perturbation: Applications to stability, sensitivity, and predictability. *Sci. China Earth Sci.*, **52**, 883–906.

—— and Zhang Rui, 2010: Is model parameter error related to a significant spring predictability barrier for El Niño event? Result from theoretical model. *Adv. Atmos. Sci.*, **27**, 1003–1013.

Frederiksen, J. S., M. Collier, and A. Watkins, 2004: Ensemble prediction of blocking regime transitions. *Tellus*, **56**, 485–500.

Jiang, Z. N., and D. H. Wang, 2010: A study on precursors to blocking anomalies in climatological flows by using conditional nonlinear optimal perturbations. *Quart. J. Roy. Meteor. Soc.*, **136**, 1170–1180.

Kamachi, M., T. Kuragano, S. Sugimoto, et al., 2004: Short-range prediction experiments with operational data assimilation system for the Kuroshio south of Japan. *J. Oceanogr.*, **60**, 269–282.

Kimoto, M., H. Mukougawa, and S. Yoden, 1992: Medium-range forecast skill variation and blocking transition: A case study. *Mon. Wea. Rev.*, **120**, 1616–1627.

Komori, N., T. Awaji, Y. Ishikawa, et al., 2003: Short-range forecast experiments of the Kuroshio path variabilities south of Japan using TOPEX/Poseidon altimetric data. *J. Geophys. Res.*, **108**(C1), 10-1-10-16.

Liu Duanling, Sun Zhaobo, and Peng Shiqiu, 2013: A study of the application of CNOP in a winter storm in the middle-lower branches of Yangtze River. *J. Trop. Meteor.*, **29**, 782–792. (in Chinese)

Marshall, J., and F. Molteni, 1993: Toward a dynamical understanding of planetary-scale flow regimes. *J. Atmos. Sci.*, **50**, 1792–1818.

Miyazawa, Y., S. Yamane, X. Y. Guo, et al., 2005: Ensemble forecast of the Kuroshio meandering. *J. Geophys. Res.*, **110**(C10), doi: 10.1029/2004JC002426.

Moore, A. M., and R. Kleeman, 1996: The dynamics of error growth and predictability in a coupled model of ENSO. *Quart. J. Roy. Meteor. Soc.*, **122**, 1405–1446.

Mu, M., 2013: Methods, current status, and prospect of targeted observation. *Sci. China Earth Sci.*, **56**, 1997–2005.

——, W. S. Duan, and B. Wang, 2003: Conditional nonlinear optimal perturbation and its applications. *Nonlinear Processes in Geophysics*, **10**, 493–501.

——, and ——, 2007a: Season-dependent dynamics of nonlinear optimal error growth and El Niño-Southern Oscillation predictability in a theoretical model. *J. Geophys. Res.*, **112**, D10113, doi: 10.1029/2005JD006981.

——, H. Xu, and W. S. Duan, 2007b: A kind of initial errors related to "spring predictability barrier" for El Niño events in Zebiak-Cane model. *Geophys. Res. Lett.*, **234**, L03709, doi: 10.1029/2006GL027412.

——, F. Zhou, and H. Wang, 2009: A method for identifying the sensitive areas in targeted observations for tropical cyclone prediction: Conditional nonlinear optimal perturbation. *Mon. Wea. Rev.*, **137**, 1623–1639.

——, and Z. Jiang, 2011: Similarities between optimal precursors that trigger the onset of blocking events and optimally growing initial errors in onset prediction. *J. Atmos. Sci.*, **68**, 2860–2877.

——, Y. S. Yu, H. Xu, et al., 2014: Similarities between optimal precursors for ENSO events and optimally growing initial errors in El Niño predictions. *Theor. Appl. Climatol.*, **115**, 461–469.

Mu Mu, Qin Xiaohao, Zhou Feifan, et al., 2012: Developing the adaptive observations, reducing the disasters. *J. Chengdu Univ. Info. Technol.*, **27**, 20–26. (in Chinese)

Qin, X. H., and M. Mu, 2011: A study on the reduction of forecast error variance by three adaptive observation approaches for tropical cyclone prediction. *Mon. Wea. Rev.*, **139**, 2218–2232.

Rex, D. F., 1950: Blocking action in the middle troposphere and its effect upon regional climate. I: An aerological study of blocking action. *Tellus*, **2**, 196–211.

Riehl, H., W. H. Haggard, and R. W. Sanborn, 1956: On the prediction of 24-hour hurricane motion. *J. Meteor.*, **13**, 415–420.

Tan Xiaowei, Wang Bin, and Wang Dongliang, 2011: Experimental studies of the impacts of the different guidances of targeting areas on the targeting observations based on the CNOP method. *Acta Meteor. Sinica*, **69**, 400–411. (in Chinese)

Tibaldi, S., and F. Molteni, 1990: On the operational predictability of blocking. *Tellus*, **42**, 343–365.

Usui, N., H. Tsujino, Y. Fujii, et al., 2006: Short-range prediction experiments of the Kuroshio path variabilities south of Japan. *Ocean Dyn.*, **56**, 607–623.

Wang Bin and Tan Xiaowei, 2009: A fast algorithm for solving CNOP and associated target observation tests. *Acta Meteor. Sinica*, **23**, 387–402.

Wang, Q., and M. Mu, 2013: The similarity between optimal precursor and optimally growing initial error in prediction of Kuroshio large meander and its application to targeted observation. *J. Geophys. Res.*, **118**, 869–884.

Wang Qiang, Mu Mu, and Dijkstra Henk, 2012: Application of the conditional nonlinear optimal perturbation method to the predictability study of the Kuroshio large meander. *Adv. Atmos. Sci.*, **29**, 118–134.

Xue, Y., M. A. Cane, and S. E. Zebiak, 1997: Predictability of a coupled model of ENSO using singular vector analysis. Part I: Optimal growth in seasonal background and ENSO cycles. *Mon. Wea. Rev.*, **125**, 2043–2056.

Yu, Y. S., W. Duan, H. Xu, et al., 2009: Dynamics of nonlinear error growth and season-dependent predictability of El Niño events in the Zebiak-Cane model. *Quart. J. Roy. Meteor. Soc.*, **135**, 2146–2160.

——, M. Mu, and W. Duan, 2012a: Does model parameter error cause a significant spring predictability barrier for El Niño events in the Zebiak-Cane model? *J. Climate*, **25**, 1263–1277.

——, ——, ——, et al., 2012b: Contribution of the location and spatial pattern of initial error to uncertainties in El Niño predictions. *J. Geophys. Res.*, **117**, C06018, doi: 10.1029/2011JC007758.

Zebiak, S. E., and M. Cane, 1987: A model El Niño-southern oscillation. *Mon. Wea. Rev.*, **115**, 2262–2278.